ELSEVIER

Chemical Engineering Journal 84 (2001) 445–461

Chemical Engineering Journal

www.elsevier.com/locate/cej

Solving design equations for a hollow fiber bioreactor with arbitrary kinetics

María I. Cabrera[1], Julio A. Luna[2], Ricardo J. Grau*[,2]

Instituto de Desarrollo Tecnológico para la Industria Química (INTEC), Universidad Nacional del Litoral and CONICET, Güemes 3450, 3000 Santa Fe, Argentina

Received 12 May 1999; received in revised form 3 October 2000; accepted 4 October 2000

Abstract

An approach for solving the hollow fiber bioreactor design equations is presented. The original set of differential mass balance equations is cast into an equivalent system of integral equations by generating the appropriate Green's functions. Mathematical features common to all hollow fiber bioreactors (HFBRs) operating with laminar flow are imbedded in the corresponding Green's functions on the lumen side, and thus separated from specific aspects arising from mass transport through the permeable wall. On the spongy matrix side, the appropriate Green's functions are expressed in terms of the mass transfer properties without involving any chemical kinetic parameters; this avoids repetitive computational effort when treating different reaction kinetics.

The derived integral equations are numerically solved on an appropriately transformed coordinate system. The numerical method is well suited for problems where steep gradients of concentration cause an inaccurate numerical integration and low rates of convergence if the equations are solved with a uniform rectangular grid on the original coordinate system. The effectiveness of the proposed approach for the simulation of HFBRs with power-law, Michaelis–Menten and zero-order kinetics is demonstrated. The method is readily extendible to treat problems with chemical kinetics described by any arbitrary functional form.

Keywords: Hollow fiber bioreactor; Design integral equations; Arbitrary kinetics; Green's functions; Iterative computation method

1. Introduction

Advances in the integration of permeable and selective membranes with biological catalysts such as live cells and enzymes provide the basis to develop competitive bioprocessing schemes. Several configurations having a bundle of hollow fibers as core of the membrane device are used in diverse applications including reverse osmosis, ultrafiltration, dialysis, and biocatalyst immobilization. After the successful use of hollow fiber bioreactors (HFBRs) for the cultivation of mammalian cells [1], HFBRs have found applications in enzymatic reactions, microbial fermentations, animal cell culture and plant cell culture [2–4].

Consequently, the design and simulation of HFBRs has been dealt with in different ways and with different levels of simplification [5]. In this regard, several papers have been written among which we can cite some of the best known fundamental contributions from the numerical solution viewpoint. Exact analytic expressions for the substrate concentration profile throughout an HFBR have been deduced for a first-order reaction rate using an integral formulation and solving Michaelis–Menten kinetics by numerical finite difference [6]. Analytic solutions have been developed in terms of Kummer functions with constants depending on the value of the Sherwood number at the permeable wall [7]. Models utilising effectiveness factors for both first- and zero-order kinetics have been developed [8]. A mathematical analysis of oxygen depletion has been performed in order to develop effectiveness factor plots to aid in the scaling of HFBRs [9]. A non-linear mixed-type problem similar to that described for HFBRs has been solved by a non-iterative finite difference method [10,11] or by an iterative fourth-order Runge–Kutta–Gill algorithm [12]. A procedure based on a Crank–Nicolson discretization has been developed to solve a generalized mathematical model for describing annular reactors and HFBRs as particular applications [13]. Methodologies for simplifying the solution of HFBR design equations have been described for the first-order and zero-order limits of the Michaelis–Menten kinetics [14,15]. Numerical solutions are required to solve zero-order kinetics with substrate exhaustion, but

* Corresponding author. Fax: +54-342-4550944.
E-mail address: cqfina@ceride.gov.ar (R.J. Grau).
[1] Member of CONICET's Research Staff.
[2] Professor at UNL and Member of CONICET's Research Staff.

1385-8947/01/$ – see front matter
PII: S1385-8947(00)00269-2

Nomenclature

a	inner radius of the membrane (cm)
A_n	normalization constant for the nth eigenfunction (dimensionless)
b	outer radius of the membrane (cm)
c	concentration (mol cm^{-3})
c	array of concentrations in the spongy matrix region (mol cm^{-3})
C	c/c^0, concentration (dimensionless)
C	array of concentrations in the spongy matrix region (dimensionless)
C_b	averaged bulk concentrations (dimensionless)
d	outer radius of the spongy matrix wall (cm)
D	diffusion coefficient of substrate (cm^2 s^{-1})
G	Green's function
Ge	a/L, geometrical parameter (dimensionless)
H	$-D^{II}K^a/D^I \ln(a/b)$, membrane mass transfer coefficient (dimensionless)
J	Jacobian
K	K^b/K^a, lumen/spongy matrix partition coefficient (dimensionless)
K^a	lumen/membrane partition coefficient (dimensionless)
K^b	membrane/spongy matrix partition coefficient (dimensionless)
K_M	Michaelis–Menten constant (mol cm^{-3})
L	hollow fiber length (cm)
L_e	entrance length (cm)
M	confluent hypergeometric function
n	reaction order
N	total number of species in the system
Pe	$V_{mx}\, a/D^I$, Peclet number (dimensionless)
r	radial coordinate (cm)
R	reaction rate (s^{-1})
Re	$2aV_{mx}\rho/\mu$, Reynolds number (dimensionless)
V_M	maximum reaction rate (s^{-1})
V_{mx}	maximum velocity (cm s^{-1})
z	axial coordinate (cm)

Greek letters

$\alpha_\zeta, \alpha_\varphi$	parameters in Eqs. (70) and (71)
β	d/b, parameter (dimensionless)
δ	Dirac delta function
ζ	dimensionless transformed axial coordinate
φ	dimensionless transformed radial coordinate
Θ	step function
λ_n	nth eigenvalue defined by Eq. (24)
μ	viscosity (P)
ν	stoichiometric coefficient
ξ	z/L (dimensionless axial coordinate)
ρ	r/a (zone I) or r/b (zone III) (dimensionless radial coordinate); density (g cm^{-3})
ϕ_n	nth eigenfunction defined by Eq. (23)
Φ	Thiele modulus, $(b^2\, V_M (c^0)^{n-1}/D^{III})^{1/2}$ for power-law kinetics, $(b^2\, V_M/K_M\, D^{III})^{1/2}$ for Michaelis–Menten kinetics, and $(b^2\, V_M/c^0 D^{III})^{1/2}$ for zero-order kinetics
Ω	$b^2 R^{III}/c^0 D^{III}$ (dimensionless reaction rate)

Superscripts

I, II, III	lumen, fiber, and spongy matrix regions, respectively
0	at the reactor inlet

Subscripts

c	at critical boundary
i	denotes component i
n	nth value

analytical solutions in terms of Kummer functions are possible for either first-order or zero-order with substrate remaining constant everywhere in the HFBR. An extension to treat first-order kinetics and power-law-type fluids has been presented [16]. A method based on the shooting technique has been proposed to avoid problems accompanying the application of the orthogonal collocation on finite elements [17]. Finite difference and orthogonal collocation methods have been used to solve dynamic models of HFBRs [18–21]. Also, the mathematical modelling of HFBRs has been reviewed with illustrative computational model calculations [5].

This work deals with the solution of the HFBR design equations for the case in which the kinetics may be described by any arbitrary function. The original set of differential balance equations with the corresponding initial and boundary conditions is turned into an equivalent system of integral equations that represents the formal solution to the original differential problem. On the lumen side, the species mass balance equation is expressed in terms of eigenfunctions whose eigenvalues do not depend on the value of the Sherwood number at the permeable wall. This is particularly advantageous since in contrast with other results once the eigenvalues are calculated, they become a set of values which is valid for all cases. On the spongy matrix side, the governing differential equation for the substrate is cast in terms of an integral equation by the definition of a Green's function which depends neither on the functional form of the kinetic equation nor on the value of the kinetic parameters. Thus, this generalized formulation is valid for any arbitrary kinetic equation, including zero-order reaction rate with substrate depleted before reaching the outer annular wall. For the last case, an unmatched expression upon the knowledge of the critical radius at any axial position is obtained in terms of characteristic parameters of the HFBR.

Efficient numerical schemes of solution are designed by means of a simple iterative process along the permeable wall and through the spongy matrix, without having to resort to

the complete concentration profiles in the lumen. Since significant concentration gradients may truly exist in HFBRs [22], it is showed that the integral equations can be solved very efficiently using a continuous coordinate transformation from a variable grid, which has a severe stretching in regions with steep changes of concentration, to another fixed one. Consequently, an improved accuracy of the solution without wasting computer memory space and running time is obtained. The computations are quite simple and faster than the one corresponding to the original integral equations. The flexibility of the proposed iterative scheme is demonstrated through its application to several types of kinetic equations. Comparative convergence maps are presented in terms of the model parameters.

For zero-order kinetics, maps to know a priori if the substrate concentration drops to zero inside the spongy matrix are given in terms of the parameters of the HFBR model. The one-dimensional free-boundary problem which arises if the substrate becomes depleted at the so-called critical radius is efficiently solved using any standard method to solve zeros of non-linear equations.

2. Assumptions and mathematical model

A schematic representation of a conventional HFBR is shown in Fig. 1, where a cross-sectional view of an individual hollow fiber in the HFBR shows three regions. Region I is the lumen (inner tube), region II is the permeable membrane (wall of the inner tube), and region III is the spongy matrix (annular region) inside which an active biocatalyst in the form of either enzymes or live cells is immobilized. The substrate solution is fed through the lumen and diffuses inside out through the permeable membrane to react by catalytic effect of active enzymes or live cells supported on the spongy matrix. The product diffuses back to the lumen and flows downstream.

The physical model for steady-state and isothermal regime includes the following simplifying assumptions: For region I: (i) laminar flow with parabolic and totally developed velocity profile, (ii) negligible axial diffusion with respect to the convective flux, (iii) Fickian diffusion in the radial direction, (iv) absence of homogeneous reaction rate in the bulk of the lumen, (v) constant physical properties. For region II: (vi) inert membrane, (vii) axial diffusion and convective flux negligible with respect to the radial diffusion, (viii) mass transfer and partition coefficients are constants. For region III: (ix) axial diffusion and convective transport are neglected in all regions, and (x) kinetics model is described by any arbitrary function of the reactant concentrations.

The governing mass balance differential equations for the ith species in each of the three regions are:

$$D_i^{\mathrm{I}}\frac{1}{r}\frac{\partial}{\partial r}\left[r\frac{\partial}{\partial r}c_i^{\mathrm{I}}(r,z)\right]-2V_{\mathrm{mx}}\left[1-\frac{r^2}{a^2}\right]\frac{\partial}{\partial z}c_i^{\mathrm{I}}(r,z)=0,\quad 0<r<a,\ \ 0<z<L \tag{1}$$

$$D_i^{\mathrm{II}}\frac{1}{r}\frac{\partial}{\partial r}\left[r\frac{\partial}{\partial r}c_i^{\mathrm{II}}(r,z)\right]=0,\quad a<r<b,\ \ 0<z<L \tag{2}$$

$$D_i^{\mathrm{III}}\frac{1}{r}\frac{\partial}{\partial r}\left[r\frac{\partial}{\partial r}c_i^{\mathrm{III}}(r,z)\right]-\nu_i R^{\mathrm{III}}(\mathbf{c}(r,z))=0,\quad b<r<d,\ \ 0<z<L \tag{3}$$

with the boundary conditions:

$$D_i^{\mathrm{I}}\frac{\partial}{\partial r}c_i^{\mathrm{I}}(0,z)=0 \tag{4}$$

$$D_i^{\mathrm{I}}\frac{\partial}{\partial r}c_i^{\mathrm{I}}(a,z)=D_i^{\mathrm{II}}\frac{\partial}{\partial r}c_i^{\mathrm{II}}(a,z)\quad\text{with}\quad K_i^a=\frac{c_i^{\mathrm{II}}(a,z)}{c_i^{\mathrm{I}}(a,z)} \tag{5}$$

$$D_i^{\mathrm{II}}\frac{\partial}{\partial r}c_i^{\mathrm{II}}(b,z)=D_i^{\mathrm{III}}\frac{\partial}{\partial r}c_i^{\mathrm{III}}(b,z)\quad\text{with}\quad K_i^b=\frac{c_i^{\mathrm{III}}(b,z)}{c_i^{\mathrm{II}}(b,z)} \tag{6}$$

$$D_i^{\mathrm{III}}\frac{\partial}{\partial r}c_i^{\mathrm{III}}(d,z)=0\quad\text{if}\quad c_i^{\mathrm{III}}(d,z)\geq 0 \tag{7a}$$

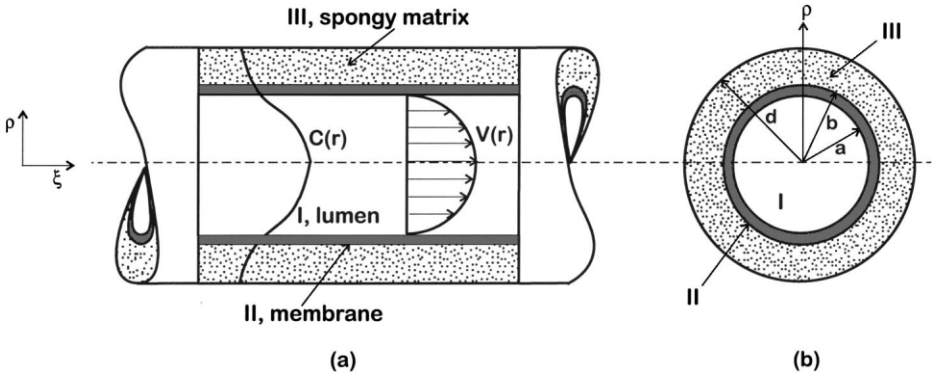

Fig. 1. Schematic diagram of the hollow fiber bioreactor with laminar velocity profile in the lumen region: (a) axial cross-section, and (b) radial cross-section.

$$D_i^{\mathrm{III}} \frac{\partial}{\partial r} c_i^{\mathrm{III}}(r_c, z) = 0 \quad \text{if } c_i^{\mathrm{III}}(r_c, z) = 0 \text{ for } b \le r_c < d \tag{7b}$$

and with the initial conditions:

$$c_i^{\mathrm{I}}(r, 0) = c_i^{\mathrm{I0}}(r) \quad \text{for } i = \text{reactant} \tag{8a}$$

$$c_i^{\mathrm{I}}(r, 0) = 0 \quad \text{for } i \neq \text{reactant} \tag{8b}$$

By using the following definitions,

$$C_i = \frac{c_i}{c_i^0} \tag{9}$$

$$\rho = \begin{cases} \dfrac{r}{a}, & \text{zone I} \\ \dfrac{r}{b}, & \text{zone III} \end{cases} \tag{10}$$

$$\xi = \frac{z}{L} \tag{11}$$

$$Ge = \frac{a}{L} \tag{12}$$

$$Pe_i = \frac{V_{\mathrm{mx}}\, a}{D_i^{\mathrm{I}}} \tag{13}$$

$$H_i = -\frac{D_i^{\mathrm{II}}}{D_i^{\mathrm{I}}} \frac{K_i^a}{\ln(a/b)} \tag{14}$$

and taking advantage of the special definition of the dimensionless radial coordinate, the mass balance equation in the membrane can be written after analytical integration as a modified boundary condition at $\rho = 1$. This boundary condition lumps the mass balance in the membrane and couples directly the dimensionless mass balance equations in the lumen and spongy matrix regions [10,14]. This is very useful for further numerical integration purposes because the number of differential equations to be solved reduces from three to two in the domain $0 \le \rho \le \beta$ and $0 \le \xi \le 1$, as follows:

$$\frac{1}{\rho}\frac{\partial}{\partial \rho}\left[\rho \frac{\partial}{\partial \rho} C_i^{\mathrm{I}}(\rho, \xi)\right] - 2\, Ge\, Pe_i [1 - \rho^2] \frac{\partial}{\partial \xi} C_i^{\mathrm{I}}(\rho, \xi) = 0, \quad 0 < \rho < 1, \ 0 < \xi < 1 \tag{15}$$

$$\frac{1}{\rho}\frac{\partial}{\partial \rho}\left[\rho \frac{\partial}{\partial \rho} C_i^{\mathrm{III}}(\rho, \xi)\right] - \nu_i \Omega^{\mathrm{III}}(\mathbf{C}(\rho, \xi)) = 0, \quad 1 < \rho < \beta, \ 0 < \xi < 1 \tag{16}$$

with boundary conditions given by

$$\left.\frac{\partial}{\partial \rho} C_i^{\mathrm{I}}(\rho, \xi)\right|_{\rho=0} = 0 \tag{17}$$

$$\left.\frac{\partial}{\partial \rho} C_i^{\mathrm{I}}(\rho, \xi)\right|_{\rho=1} - H_i [C_i^{\mathrm{I}}(1, \xi) - K_i C_i^{\mathrm{III}}(1, \xi)] = 0 \tag{18}$$

$$\left.\frac{\partial}{\partial \rho} C_i^{\mathrm{III}}(\rho, \xi)\right|_{\rho=\beta} = 0 \quad \text{if } C_i^{\mathrm{III}}(\beta, \xi) \ge 0 \tag{19a}$$

$$\left.\frac{\partial}{\partial \rho} C_i^{\mathrm{III}}(\rho, \xi)\right|_{\rho=\rho_c} = 0 \quad \text{if } C_i^{\mathrm{III}}(\rho_c, \xi) = 0 \text{ for } 1 \le \rho_c < \beta \tag{19b}$$

and with the following initial condition:

$$C_i^{\mathrm{I}}(\rho, 0) = C_i^{\mathrm{I0}}(\rho) \quad \text{for } i = \text{reactant} \tag{20a}$$

$$C_i^{\mathrm{I}}(\rho, 0) = 0 \quad \text{for } i \neq \text{reactant} \tag{20b}$$

Eq. (18) lumps the mass balance in the membrane. Eqs. (19a) and (19b) account for either the fixed boundary value problem or the free boundary value problem arising for certain kinetic models. As a complete depletion of substrate cannot occur for all non zero-order reaction rates, then Eq. (19a) is always fulfilled for non zero-order kinetic models [13,15]. However, two situations can be identified for the zero-order reaction rate: (a) the substrate concentration does not become zero at any point within the spongy matrix, thus Eq. (19a) is ultimately fulfilled; and (b) the substrate concentration drops to zero at some point ρ_c within the spongy matrix, thus Eq. (19b) must be satisfied instead of Eq. (19a). The boundary value problem with Eq. (19b) is known as a free boundary problem because the location at which the substrate becomes depleted, ρ_c, is not previously known.

All these boundary conditions are taken into consideration because there is no restriction on the functional form of the dimensionless kinetic equation to be specified for each particular application. The most general case of non-linear kinetics model will be mathematically treated by setting $\Omega^{\mathrm{III}}(\mathbf{C}(\rho, \xi))$ as any arbitrary function of the species concentrations, $\mathbf{C}(C_1^{\mathrm{III}}, \ldots, C_i^{\mathrm{III}}, \ldots, C_N^{\mathrm{III}})$. As a particular case, the solution for zero-order kinetics will be derived from the general solution to be obtained further on.

For simplicity, from now on the subindex i will be dropped from the dimensionless parameters and concentration of the ith species.

3. Design equations in terms of integral equations

3.1. Lumen region

To transform differential mass balance equations, like to Eq. (15), into their equivalent integral equations we have successfully applied an approach which consists of four steps: (1) define an appropriate differential problem for Green's function which leads to a suitable form of the formal integral solution, (2) identify Green's function by comparing the expression of the formal solution with that corresponding to its generalized Fourier expansion, (3) solve the associated homogeneous eigenvalue problem, and finally, (4) overcome the difficulty introduced by the fact that any function with

simple jump discontinuities cannot be uniformly approximated by a Fourier series in an interval close to the discontinuity (problem known as Gibbs phenomenon), as it is the case with the non-homogeneous boundary condition given by Eq. (18). This approach was used to solve the design equations for mass transfer in dialyzers [23], in packed-bed with adsorption at the wall and bulk reaction [24], in tubular reactors with heterogeneous reactions [25–28], and for reactive systems involving Couette flows [29,30].

Because Eqs. (15), (17) and (18) are quite similar to those treated in previous contributions, we need not present details of the transformation to the corresponding integral equation and shall write only the resulting final expression [23,25,26,28,31]:

$$C^{\mathrm{I}}(\rho,\xi) = \left[\sum_{1}^{\infty}\frac{\phi_n(1)\phi_n(\rho)}{A_n^2\lambda_n^2} - (\rho^2 - \frac{1}{4}\rho^4 - \frac{7}{24})\right] \times H[C^{\mathrm{I}}(1,\xi) - KC^{\mathrm{III}}(1,\xi)] + \int_0^1 \mathrm{d}\bar{\rho}\,\bar{\rho}(1-\bar{\rho}^2)G^{\mathrm{I}}(\rho,\xi/\bar{\rho},0)C^{\mathrm{I}}(\bar{\rho},0) - \frac{1}{2\,Ge\,Pe}\int_0^{\xi}\mathrm{d}\bar{\xi}\,G^{\mathrm{I}}(\rho,\xi/1,\bar{\xi})H[C^{\mathrm{I}}(1,\bar{\xi}) - KC^{\mathrm{III}}(1,\bar{\xi})] \quad (21)$$

On the right-hand side of Eq. (21), the first term accounts for the non-zero gradients at the permeable wall imposed by the non-homogeneous boundary condition at $\rho = 1$; the second term can be identified as the contribution of the inlet condition, and the last one takes into account the species mass transfer through the permeable wall [23,25,26].

Green's function is the following Fourier expansion [31]:

$$G^{\mathrm{I}}(\rho,\xi/\bar{\rho},\bar{\xi}) = \sum_{0}^{\infty}A_n^{-2}\exp\left[-\frac{\lambda_n^2}{2\,Ge\,Pe}(\xi-\bar{\xi})\right] \times\phi_n(\rho)\phi_n(\bar{\rho})\Theta(\xi-\bar{\xi}) \quad (22)$$

where $\phi_n(\rho)$ and λ_n are orthogonal eigenfunctions and eigenvalues, respectively, given by

$$\phi_n(\rho) = \exp\left[-\frac{\lambda_n\rho^2}{2}\right]M\left(\frac{2-\lambda_n}{4},1,\lambda_n\rho^2\right) \quad (23)$$

$$\lambda_n\left\{\left[1-\frac{\lambda_n}{2}\right]M\left(\frac{6-\lambda_n}{4},2,\lambda_n\right) - M\left(\frac{2-\lambda_n}{4},1,\lambda_n\right)\right\} = 0 \quad (24)$$

with A_n^2 normalization coefficients defined by

$$\int_0^1 \mathrm{d}\bar{\rho}\,\bar{\rho}(1-\bar{\rho}^2)\phi_n(\bar{\rho})\phi_m(\bar{\rho}) = A_n^2\delta_{nm} \quad (25)$$

where M is Kummer's function [32] and δ_{nm} is the Kronecker delta.

To calculate the numerical values of $C^{\mathrm{I}}(\rho,\xi)$ using Eq. (21), it is necessary to know beforehand the axial concentration profile at the permeable wall. According to Eq. (21) for $\rho = 1$, such concentration profile may be obtained by a simple iterative scheme at the wall using:

$$C^{\mathrm{I}}(1,\xi) = \left[\sum_{1}^{\infty}\frac{\phi_n(1)\phi_n(1)}{A_n^2\lambda_n^2} - \frac{11}{24}\right]H[C^{\mathrm{I}}(1,\xi) - KC^{\mathrm{III}}(1,\xi)] + \int_0^1 \mathrm{d}\bar{\rho}\,\bar{\rho}(1-\bar{\rho}^2)G^{\mathrm{I}}(1,\xi/\bar{\rho},0)C^{\mathrm{I}}(\bar{\rho},0) - \frac{1}{2\,Ge\,Pe}\int_0^{\xi}\mathrm{d}\bar{\xi}\,G^{\mathrm{I}}(1,\xi/1,\bar{\xi})H[C^{\mathrm{I}}(1,\bar{\xi}) - KC^{\mathrm{III}}(1,\bar{\xi})] \quad (26)$$

where the values of $C^{\mathrm{III}}(1,\xi)$ may also be evaluated quickly by using a simple iterative scheme based on the integral equation to be immediately deduced for the substrate in the spongy matrix.

3.2. Spongy matrix region

If the substrate concentration does not become depleted at some intermediate position in the reactor annulus, the handling of spatial discontinuities imposed by the boundary conditions is straightforward because their location is fixed (Case (a)). The problem becomes more difficult to handle if the substrate concentration drops to zero at some point ρ_{c} within the spongy matrix region. In such case, only the zone $1 < \rho < \rho_{\mathrm{c}}$ is effective for reaction and, therefore, Eq. (16) must be solved in the space domain with substrate concentration greater than zero (Case (b)). Both cases are treated systematically as follows.

As a starting point, the governing local equation for the substrate concentration is advantageously expressed as a local field equation which is entirely valid in the whole annular space even if the substrate concentration is not finite everywhere inside the reactor annulus. For such purpose, an indicator function is defined as

$$\Theta(\rho_{\mathrm{c}}-\rho) = \begin{cases} 1 & \text{if } \rho_{\mathrm{c}} \geq \rho \\ 0 & \text{if } \rho_{\mathrm{c}} < \rho \end{cases} \quad (27)$$

$\Theta(\rho_{\mathrm{c}}-\rho)$ being a Heaviside step function whose derivative is given by

$$\frac{\mathrm{d}}{\mathrm{d}\rho}\Theta(\rho_{\mathrm{c}}-\rho) = -\delta(\rho_{\mathrm{c}}-\rho) \quad (28)$$

where $\delta(\rho_{\mathrm{c}}-\rho)$ is the generalized delta function [33].

Using the indicator function as follows:

$$\Theta(\rho_{\mathrm{c}}-\rho)\left\{\frac{1}{\rho}\frac{\partial}{\partial\rho}\left[\rho\frac{\partial}{\partial\rho}C^{\mathrm{III}}(\rho,\xi)\right] - \nu\Omega^{\mathrm{III}}(\mathbf{C}(\rho,\xi))\right\} = 0, \quad 1<\rho<\beta, \quad 0<\xi<1 \quad (29)$$

the governing differential equation for substrate concentration can be now expressed as

$$\frac{1}{\rho}\frac{\partial}{\partial\rho}\left\{\rho\frac{\partial}{\partial\rho}[\Theta(\rho_c-\rho)C^{III}(\rho,\xi)]\right\} -\Theta(\rho_c-\rho)\nu\Omega^{III}(\mathbf{C}(\rho,\xi)) = -\delta(\rho_c-\rho)\frac{\partial}{\partial\rho}C^{III}(\rho,\xi) -\frac{1}{\rho}\frac{\partial}{\partial\rho}[\rho\delta(\rho_c-\rho)C^{III}(\rho,\xi)], \quad 1<\rho<\beta,\ \ 0<\xi<1 \tag{30}$$

which, unlike Eq. (16), is a field equation because it is valid in all the space domain occupied by the spongy matrix.

Thus, in turn, the boundary conditions given by Eqs. (18) and (19a) become

$$\frac{\partial}{\partial\rho}[\Theta(\rho_c-\rho)C^{I}(\rho,\xi)]\bigg|_{\rho=1} + H[\Theta(\rho_c-1)C^{I}(1,\xi) -K\Theta(\rho_c-1)C^{III}(1,\xi)] = \delta(\rho_c-1)C^{III}(1,\xi) \tag{31}$$

$$\frac{\partial}{\partial\rho}[\Theta(\rho_c-\rho)C^{III}(\rho,\xi)] - \delta(\rho_c-\rho)C^{III}(\rho,\xi)\bigg|_{\rho=\beta\text{ or }\rho_c} = 0 \tag{32}$$

One may notice that if there is total depletion of the substrate, local sources arise from the discontinuity at $\rho=\rho_c$. Otherwise, Eqs. (30)–(32) become Eqs. (16), (18), (19a) and (19b). In accordance with the properties of a Dirac function, these field equations have full significance under an integral operator.

To obtain the integral formal solution, an integration of Eq. (30) is performed with ρ as weight function and with a test function $G^{III}(\rho/\bar\rho)$, still unspecified, as follows:

$$\int_1^\beta \mathrm{d}\bar\rho\, G^{III}(\rho/\bar\rho)\frac{\partial}{\partial\bar\rho}\left\{\bar\rho\frac{\partial}{\partial\bar\rho}[\Theta(\rho_c-\bar\rho)C^{III}(\bar\rho,\xi)]\right\} = +\nu\int_1^\beta \mathrm{d}\bar\rho\,\bar\rho G^{III}(\rho/\bar\rho)\Theta(\rho_c-\bar\rho)\Omega^{III}(\mathbf{C}(\bar\rho,\xi)) -\int_1^\beta \mathrm{d}\bar\rho\,\bar\rho G^{III}(\rho/\bar\rho)\delta(\rho_c-\bar\rho)\frac{\partial}{\partial\bar\rho}C^{III}(\bar\rho,\xi) -\int_1^\beta \mathrm{d}\bar\rho\, G^{III}(\rho/\bar\rho)\frac{\partial}{\partial\bar\rho}[\bar\rho\delta(\rho_c-\bar\rho)C^{III}(\bar\rho,\xi)] \tag{33}$$

Successive integrations by parts on the left-hand side of Eq. (33), followed by some rearrangements taking into account Eqs. (31) and (32), lead to the following equation:

$$\int_1^\beta \mathrm{d}\bar\rho\,\Theta(\rho_c-\bar\rho)C^{III}(\bar\rho,\xi)\frac{\partial}{\partial\bar\rho}\left\{\bar\rho\frac{\partial}{\partial\bar\rho}G^{III}(\rho/\bar\rho)\right\} = +\nu\int_1^\beta \mathrm{d}\bar\rho\,\bar\rho G^{III}(\rho/\bar\rho)\Theta(\rho_c-\bar\rho)\Omega^{III}(\mathbf{C}(\bar\rho,\xi)) +\Theta(\rho_c-1)C^{III}(1)\ \frac{\partial}{\partial\bar\rho}G^{III}(\rho/\bar\rho)\bigg|_{\bar\rho=1} -\Theta(\rho_c-1)G^{III}(\rho/1)\ \frac{\partial}{\partial\bar\rho}C^{III}(\bar\rho,\xi)\bigg|_{\bar\rho=1} -\beta\Theta(\rho_c-\beta)C^{III}(\beta)\ \frac{\partial}{\partial\bar\rho}G^{III}(\rho/\bar\rho)\bigg|_{\bar\rho=\beta} +\Theta(\rho_c-\beta)G^{III}(\rho/\beta)\ \frac{\partial}{\partial\bar\rho}C^{III}(\bar\rho,\xi)\bigg|_{\bar\rho=\beta} +\int_1^\beta \mathrm{d}\bar\rho\,\bar\rho C^{III}(\bar\rho)\frac{\partial}{\partial\bar\rho}G^{III}(\rho/\bar\rho)\delta(\rho_c-\bar\rho) -\int_1^\beta \mathrm{d}\bar\rho\,\bar\rho G^{III}(\rho/\bar\rho)\frac{\partial}{\partial\bar\rho}C^{III}(\bar\rho,\xi)\delta(\rho_c-\bar\rho) \tag{34}$$

which reduces as follows:

1. For the Case (a) as $\rho_c \geq \beta$, then

$$\Theta(\rho_c-\beta)=1 \tag{35}$$

and

$$\delta(\rho_c-\bar\rho)=0 \quad \text{for}\ \ 1\leq\bar\rho\leq\beta \tag{36}$$

thus Eq. (34) becomes

$$\int_1^\beta \mathrm{d}\bar\rho\,\Theta(\rho_c-\bar\rho)C^{III}(\bar\rho,\xi)\frac{\partial}{\partial\bar\rho}\left\{\bar\rho\frac{\partial}{\partial\bar\rho}G^{III}(\rho/\bar\rho)\right\} = +\nu\int_1^\beta \mathrm{d}\bar\rho\,\bar\rho G^{III}(\rho/\bar\rho)\Theta(\rho_c-\bar\rho)\Omega^{III}(\mathbf{C}(\bar\rho,\xi)) +\Theta(\rho_c-1)C^{III}(1)\ \frac{\partial}{\partial\bar\rho}G^{III}(\rho/\bar\rho)\bigg|_{\bar\rho=1} -\Theta(\rho_c-1)G^{III}(\rho/1)\ \frac{\partial}{\partial\bar\rho}C^{III}(\bar\rho,\xi)\bigg|_{\bar\rho=1} -\beta\Theta(\rho_c-\beta)C^{III}(\beta)\ \frac{\partial}{\partial\bar\rho}G^{III}(\rho/\bar\rho)\bigg|_{\bar\rho=\beta} +\Theta(\rho_c-\beta)G^{III}(\rho/\beta)\ \frac{\partial}{\partial\bar\rho}C^{III}(\bar\rho,\xi)\bigg|_{\bar\rho=\beta} \tag{37}$$

2. For the Case (b) as $\rho_c < \beta$, then

$$\Theta(\rho_c-\beta)=0 \tag{38}$$

and taking into account the following property of the delta function,

$$\int_1^\beta \mathrm{d}\bar\rho\, F(\bar\rho)\delta(\rho_c-\bar\rho) = -F(\rho_c) \tag{39}$$

Eq. (34) becomes

$$\int_1^\beta \mathrm{d}\bar{\rho}\,\Theta(\rho_c-\bar{\rho})C^{III}(\bar{\rho},\xi)\frac{\partial}{\partial\bar{\rho}}\left\{\bar{\rho}\frac{\partial}{\partial\bar{\rho}}G^{III}(\rho/\bar{\rho})\right\}$$
$$=+\nu\int_1^\beta \mathrm{d}\bar{\rho}\,\bar{\rho}G^{III}(\rho/\bar{\rho})\Theta(\rho_c-\bar{\rho})\Omega^{III}(\mathbf{C}(\bar{\rho},\xi))$$
$$+\Theta(\rho_c-1)C^{III}(1)\left.\frac{\partial}{\partial\bar{\rho}}G^{III}(\rho/\bar{\rho})\right|_{\bar{\rho}=1}$$
$$-\Theta(\rho_c-1)G^{III}(\rho/1)\left.\frac{\partial}{\partial\bar{\rho}}C^{III}(\bar{\rho},\xi)\right|_{\bar{\rho}=1}$$
$$+\rho_c C^{III}(\rho_c)\left.\frac{\partial}{\partial\bar{\rho}}G^{III}(\rho/\bar{\rho})\right|_{\bar{\rho}=\rho_c}$$
$$-\rho_c G^{III}(\rho/\rho_c)\left.\frac{\partial}{\partial\bar{\rho}}C^{III}(\bar{\rho},\xi)\right|_{\bar{\rho}=\rho_c} \quad (40)$$

Upon examining Eqs. (37) and (40), the convenience of requiring that $G^{III}(\rho/\bar{\rho})$ should be the solution of the problem

$$\frac{\partial}{\partial\bar{\rho}}\left[\bar{\rho}\frac{\partial}{\partial\bar{\rho}}G^{III}(\rho/\bar{\rho})\right]=-\delta(\rho-\bar{\rho}) \quad (41)$$

$$\left.\frac{\partial}{\partial\bar{\rho}}G^{III}(\rho/\bar{\rho})\right|_{\bar{\rho}=1}-HKG^{III}(\rho/1)=0 \quad (42)$$

$$\left.\frac{\partial}{\partial\bar{\rho}}G^{III}(\rho/\bar{\rho})\right|_{\bar{\rho}=\beta\text{ or }\rho_c}=0 \quad (43)$$

is apparent.

By substitution of Eqs. (41)–(43), together with Eqs. (18), (19a) and (19b), into Eqs. (37) and (40), we obtain the following formal solutions:

1. For the Case (a)

$$C^{III}(\rho,\xi)=G^{III}(\rho/1)H\Theta(\beta-\rho)C^{I}(1,\xi)$$
$$+\nu\int_1^\beta \mathrm{d}\bar{\rho}\,\bar{\rho}G^{III}(\rho/\bar{\rho})\Theta(\beta-\bar{\rho})$$
$$\times\Omega^{III}(\mathbf{C}(\bar{\rho},\xi)) \quad (44)$$

2. For the Case (b)

$$C^{III}(\rho,\xi)=G^{III}(\rho/1)\Theta(\rho_c-1)HC^{I}(1,\xi)$$
$$+\nu\int_1^\beta \mathrm{d}\bar{\rho}\,\bar{\rho}G^{III}(\rho/\bar{\rho})\Theta(\rho_c-\bar{\rho})$$
$$\Omega^{III}(\mathbf{C}(\bar{\rho},\xi)) \quad (45)$$

thus, the critical concentration of substrate at $\rho=1$ for which the concentration just becomes zero at $\rho=\rho_c$ is given by

$$C^{I}(1,\xi)=\frac{-\nu}{G^{III}(\rho_c/1)H}\int_1^\beta \mathrm{d}\bar{\rho}\,\bar{\rho}$$
$$G^{III}(\rho_c/\bar{\rho})\Theta(\rho_c-\bar{\rho})\Omega^{III}(\mathbf{C}(\bar{\rho},\xi)) \quad (46)$$

Therefore, Eqs. (44) and (46) allow us to recast the original problem for $C^{III}(\rho,\xi)$ in the form of integral equations whose terms account for the mass transfer through the permeable wall and the chemical reaction in the spongy matrix contributions. Although Green's function has been characterized by Eqs. (41)–(43), it still has to be calculated.

The identification of Green's function $G^{III}(\rho/\bar{\rho})$ is performed through a procedure quite similar to those which have been applied in previous works [27,34]. The general solution of Eq. (41) is

$$G^{III}(\rho/\bar{\rho})=[A_1+B_1\ln\bar{\rho}]\Theta(\rho-\bar{\rho})$$
$$+[A_2+B_2\ln\bar{\rho}]\Theta(\bar{\rho}-\rho) \quad (47)$$

where $\Theta(\rho-\bar{\rho})$ and $\Theta(\bar{\rho}-\rho)$ are step functions, and A_1, B_1, A_2 and B_2 are coefficients to be determined from the following four additional conditions.

A first condition is obtained by integration of Eq. (41) over the $\rho-\varepsilon$ to $\rho+\varepsilon$ range,

$$\left.\bar{\rho}\frac{\partial}{\partial\bar{\rho}}G^{III}(\rho/\bar{\rho})\right|_{\bar{\rho}=\rho-\varepsilon}^{\bar{\rho}=\rho+\varepsilon}=-1 \quad (48)$$

A second condition is provided by the continuity condition of Green's function for any $\bar{\rho}\neq\rho$,

$$G^{III}(\rho/\bar{\rho}+\varepsilon)=G^{III}(\rho/\bar{\rho}-\varepsilon) \quad (49)$$

ε being a small positive quantity. The third and fourth conditions are the previously introduced boundary conditions given by Eqs. (42) and (43).

Applying these four conditions to Eq. (47), the expression of Green's function $G^{III}(\rho/\bar{\rho})$ finally becomes

$$G^{III}(\rho/\bar{\rho})=\left[\frac{1}{HK}+\ln\bar{\rho}\right]\Theta(\rho-\bar{\rho})$$
$$+\left[\frac{1}{HK}+\ln\rho\right]\Theta(\bar{\rho}-\rho) \quad (50)$$

Substitution of Eq. (50) into Eqs. (44)–(46) defines the integral equations to describe the substrate concentration in the spongy matrix region with kinetics equation $\Omega^{III}(\mathbf{C}(\rho,\xi))$ to be described by any arbitrary function.

Coupled equations given by Eq. (21) and either Eq. (44) or Eqs. (45) and (46) are formal integral solutions which fulfil all conditions stated in the original mass balance of species in the lumen and spongy matrix regions, respectively. Green's functions defined by Eqs. (22) and (50) are fundamental ingredients for the determination of the limiting form of the general solution and to devise efficient numerical schemes of solution.

Fig. 2 shows the response surface described by the kernels of the aforementioned integral equations for $\bar{\rho}=1$ and three values of the Thiele modulus for zero-order kinetics. It may be noticed that the response surface drops to zero as long as the radial position surpasses the critical radius which is a function of the axial position. It is also evident that by increasing the Thiele modulus, the region where the response level is zero also increases.

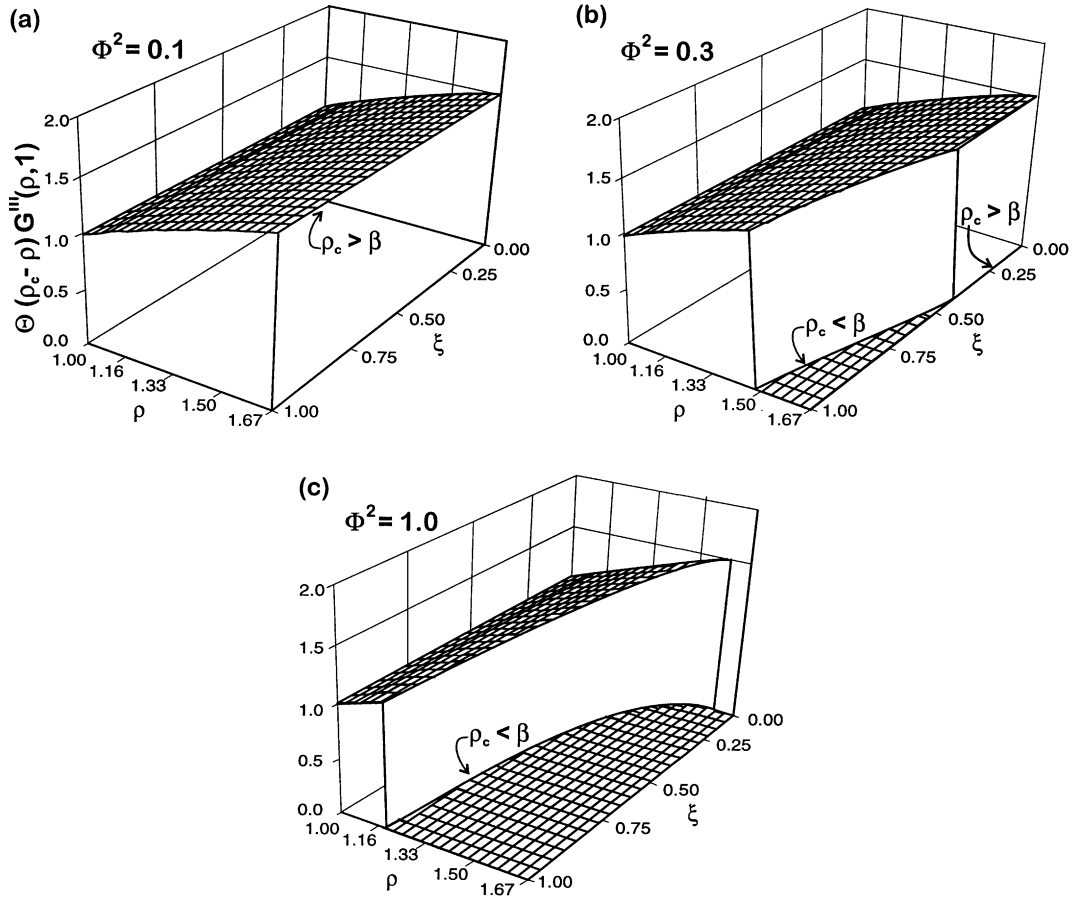

Fig. 2. Response surfaces described by the kernel of Eq. (45) for zero-order kinetics: (a) $\Phi^2 = 0.1$, (b) $\Phi^2 = 0.3$, and (c) $\Phi^2 = 1.0$ ($D^{\mathrm{I}} = 1.0 \times 10^{-5}\,\mathrm{cm^2\,s^{-1}}$, $D^{\mathrm{II}} = 4.9 \times 10^{-7}\,\mathrm{cm^2\,s^{-1}}$, $GePe = 0.5$, $K^a = 1$, $K^b = 1$, $a = 1.00 \times 10^{-2}\,\mathrm{cm}$, $b = 1.05 \times 10^{-2}\,\mathrm{cm}$, $d = 1.75 \times 10^{-2}\,\mathrm{cm}$, $L = 2 \times 10^{1}\,\mathrm{cm}$).

4. Simplified models

4.1. Uniform concentration at the inlet of the lumen region

In case the substrate concentration be assumed uniform at the lumen inlet, the first integral term on the right-hand side of Eq. (21) simplifies to 1 [23,31]. Thus Eq. (21) becomes

$$C^{\mathrm{I}}(\rho,\xi) = 1 + \left[\sum_{1}^{\infty} \frac{\phi_n(1)\phi_n(\rho)}{A_n^2\lambda_n^2} - (\rho^2 - \frac{1}{4}\rho^4 - \frac{7}{24})\right] \times H[C^{\mathrm{I}}(1,\xi) - KC^{\mathrm{III}}(1,\xi)] - \frac{1}{2\,GePe}\int_0^{\xi} \mathrm{d}\bar{\xi}\; G^{\mathrm{I}}(\rho,\xi/1,\bar{\xi}) H[C^{\mathrm{I}}(1,\bar{\xi}) - KC^{\mathrm{III}}(1,\bar{\xi})] \quad (51)$$

and the averaged bulk concentration defined by

$$C_{\mathrm{b}}^{\mathrm{I}}(\xi) = 4\int_0^1 \mathrm{d}\bar{\rho}\;\bar{\rho}(1-\bar{\rho}^2)C^{\mathrm{I}}(\bar{\rho},\xi) \quad (52)$$

can be conveniently expressed as

$$C_{\mathrm{b}}^{\mathrm{I}}(\xi) = 1 - \frac{2}{GePe}\int_0^{\xi} \mathrm{d}\bar{\xi}\; H[C^{\mathrm{I}}(1,\bar{\xi}) - KC^{\mathrm{III}}(1,\bar{\xi})] \quad (53)$$

which has a more convenient format than Eq. (52) because the numerical value of $C_{\mathrm{b}}^{\mathrm{I}}(\xi)$ may be obtained only from concentration profiles at the permeable wall, without having to solve complete concentration profiles in the lumen bulk.

4.2. Zero-order kinetics with substrate concentration remaining greater than zero throughout the spongy matrix (Case (a))

The non-dimensional kinetic expression for zero-order reaction rate is

$$\Omega^{\mathrm{III}}(\mathbf{C}(\rho,\xi)) = \Phi^2, \quad 1 < \rho < \beta, \;\; 0 < \xi < 1 \quad (54)$$

where Φ^2 is the Thiele number defined as the ratio between the diffusive mass transport and the chemical reaction characteristic times in the spongy matrix region.

By integration of Eq. (44) with Eqs. (50) and (54), we obtain the following explicit expression:

$$C^{\mathrm{III}}(\rho,\xi) = \frac{1}{K}C^{\mathrm{I}}(1,\xi) + \nu\Phi^2\left\{\frac{1}{2HK}[\beta^2-1]-\frac{1}{4}[\rho^2-1]+\frac{\beta^2}{2}\ln\rho\right\} \tag{55}$$

from which the $C^{\mathrm{III}}(\rho,\xi)$ profile can be readily obtained once the $C^{\mathrm{I}}(1,\xi)$ profile is available. From Eq. (55), it immediately follows that the impulsive force for the mass transfer between the lumen and spongy matrix sides is

$$H[C^{\mathrm{I}}(1,\xi) - KC^{\mathrm{III}}(1,\xi)] = -\tfrac{1}{2}\nu(\beta^2-1)\Phi^2 \tag{56}$$

Then, substituting this relationship into Eq. (51), it becomes

$$C^{\mathrm{I}}(\rho,\xi) = 1+\nu\Phi^2\frac{\beta^2-1}{2}\left\{\rho^2-\frac{1}{4}\rho^4-\frac{7}{24}+\frac{2}{Ge\,Pe}\xi - \sum_1^\infty \frac{\phi_n(\rho)\phi_n(1)}{A_n^2\lambda_n^2}\exp\left(-\frac{\lambda_n^2}{2\,Ge\,Pe}\xi\right)\right\} \tag{57}$$

from which, for $\rho = 1$, we obtain

$$C^{\mathrm{I}}(1,\xi) = 1+\nu\Phi^2\frac{\beta^2-1}{2}\left\{\frac{11}{24}+\frac{2}{Ge\,Pe}\xi - \sum_1^\infty \frac{\phi_n^2(1)}{A_n^2\lambda_n^2}\exp\left(-\frac{\lambda_n^2}{2\,Ge\,Pe}\xi\right)\right\} \tag{58}$$

The uncoupled Equations (57) and (58) have validity whenever the substrate concentration at the permeable wall is greater than the critical concentration for which the concentration just depletes at the shell wall, that is whenever the condition

$$C^{\mathrm{I}}(1,\xi) \geq -\nu\Phi^2 \times\left\{\frac{1}{2H}[\beta^2-1]-\frac{K}{4}[\beta^2-1]+\frac{\beta^2 K}{2}\ln\beta\right\} \tag{59}$$

is satisfied. This result provides a lower bound for the substrate concentration at the lumen wall above which the boundary condition given by Eqs. (19a) and (19b) has full validity.

4.3. Zero-order kinetics with substrate depleted before reaching the shell wall (Case (b))

So long as the reaction rate is zero if the substrate concentration drops to zero, the non-dimensional kinetic equation can be formally expressed as

$$\Omega^{\mathrm{III}}(\mathbf{C}(\rho,\xi)) = \Theta(\rho_{\mathrm{c}}-\rho)\Phi^2, \quad 1<\rho<\beta,\ \ 0<\xi<1 \tag{60}$$

Substitution of Eq. (60) into Eq. (45) followed by integration using Eq. (50) gives

$$C^{\mathrm{III}}(\rho,\xi) = \Theta(\rho_{\mathrm{c}}-1)\frac{1}{K}C^{\mathrm{I}}(1,\xi)+\Theta(\rho_{\mathrm{c}}-\rho)\nu\Phi^2 \times\left\{\frac{1}{2HK}[\rho_{\mathrm{c}}^2-1]-\frac{1}{4}[\rho^2-1]+\frac{\rho_{\mathrm{c}}^2}{2}\ln\rho\right\} \tag{61}$$

from which the $C^{\mathrm{I}}(1,\xi)$ profile can be easily obtained invoking the substrate depletion just at $\rho=\rho_{\mathrm{c}}$, thus:

$$C^{\mathrm{I}}(1,\xi) = -\nu\Phi^2 K\left\{\frac{1}{2HK}[\rho_{\mathrm{c}}^2-1]-\frac{1}{4}[\rho_{\mathrm{c}}^2-1]+\frac{\rho_{\mathrm{c}}^2}{2}\ln\rho_{\mathrm{c}}\right\} \tag{62}$$

Substitution of Eq. (62) into Eq. (61) leads to a simple equation which describes the substrate concentration profile in the spongy matrix region:

$$C^{\mathrm{III}}(\rho,\xi) = \Theta(\rho_{\mathrm{c}}-\rho)\nu\Phi^2\left\{\frac{1}{4}[\rho_{\mathrm{c}}^2-\rho^2]+\frac{\rho_{\mathrm{c}}^2}{2}\ln\frac{\rho}{\rho_{\mathrm{c}}}\right\} \tag{63}$$

where ρ_{c} remains still unspecified. Then, from Eqs. (60)–(63) comes out the need for the knowledge of the critical radius ρ_{c}.

An additional condition to be satisfied by ρ_{c} comes from Eq. (55) evaluated at $\rho=1$:

$$H[C^{\mathrm{I}}(1,\xi) - KC^{\mathrm{III}}(1,\xi)] = -\tfrac{1}{2}\nu(\rho_{\mathrm{c}}^2-1)\Phi^2 \tag{64}$$

Then, substitution of Eq. (64) into Eq. (51), after integration, yields

$$C^{\mathrm{I}}(\rho,\xi) = 1+\nu\Phi^2\frac{\rho_{\mathrm{c}}^2-1}{2}\left\{\rho^2-\frac{1}{4}\rho^4-\frac{7}{24}+\frac{2}{Ge\,Pe}\xi - \sum_1^\infty \frac{\phi_n(\rho)\phi_n(1)}{A_n^2\lambda_n^2}\exp\left(-\frac{\lambda_n^2}{2\,Ge\,Pe}\xi\right)\right\} \tag{65}$$

which for $\rho=1$ becomes

$$C^{\mathrm{I}}(1,\xi) = 1+\nu\Phi^2\frac{\rho_{\mathrm{c}}^2-1}{2}\left\{\frac{11}{24}+\frac{2}{Ge\,Pe}\xi - \sum_1^\infty \frac{\phi_n^2(1)}{A_n^2\lambda_n^2}\exp\left(-\frac{\lambda_n^2}{2\,Ge\,Pe}\xi\right)\right\} \tag{66}$$

Finally, by linking Eqs. (62) and (66), it results that

$$0 = 1+\nu\Phi^2 K\left\{\frac{1}{2HK}[\rho_{\mathrm{c}}^2-1]-\frac{1}{4}[\rho_{\mathrm{c}}^2-1]+\frac{\rho_{\mathrm{c}}^2}{2}\ln\rho_{\mathrm{c}}\right\} +\nu\Phi^2\frac{\rho_{\mathrm{c}}^2-1}{2}\left\{\frac{11}{24}+\frac{2}{Ge\,Pe}\xi - \sum_1^\infty \frac{\phi_n^2(1)}{A_n^2\lambda_n^2}\exp\left(-\frac{\lambda_n^2}{2\,Ge\,Pe}\xi\right)\right\} \tag{67}$$

from which the critical radius can be numerically obtained as a function of the axial position.

As a limiting case of this generalized formulation, Eq. (67) provides an unmatched expression upon the knowledge of the critical radius as a function of the axial position and the diffusive-to-convective (Pe) and diffusive-to-reaction (Φ^2) characteristic times ratios, the partitioning parameters (K), the mixed parameters (H), and the geometrical ratio (Ge) of the HFBR. The values of the critical radius can be obtained according to Eq. (67) by application of any standard method to solve zeros of a system of nonlinear equations. Then, once the values of the critical radius are known, the substrate concentration profiles in the active matrix and lumen regions can be straightaway obtained from Eqs. (63) and (65), respectively, without having to resort to an iterative scheme of numerical solution.

5. Numerical solution

5.1. Numerical algorithm

The concentration profiles of substrate at the membrane wall on the lumen side can be obtained from Eq. (26), and on the spongy matrix from Eq. (44) evaluated at $\rho = 1$. Then the proposed iterative procedure to obtain the solution proceeds as follows: (i) assume values for the concentration profiles on the boundary at $\rho = 1$; (ii) solve Eq. (26) according to the sequence:

$$C^{\mathrm{I}}(1,\xi)^{j+1} = F[C^{\mathrm{III}}(1,\xi), C^{\mathrm{I}}(1,\xi)^{j}] \tag{68}$$

until the resulting axial profile has the desired accuracy; (iii) solve Eq. (44) with the result obtained in step (ii) following the sequence:

$$C^{\mathrm{III}}(\rho,\xi)^{k+1} = F[C^{\mathrm{I}}(1,\xi), C^{\mathrm{III}}(\rho,\xi)^{k}] \tag{69}$$

until the resulting radial profile has the desired accuracy; (iv) evaluate $C^{\mathrm{III}}(1,\xi)$ from the values obtained in step (iii) and compare with the old profile assumed in step (i); and (v) proceed with the iterative scheme until each value of $C^{\mathrm{III}}(1,\xi)$ calculated between two consecutive steps of overall iteration has a relative error smaller than the prescribed value. Thus, the iterative process proceeds on the boundary at $\rho = 1$ and throughout the spongy matrix, without having to solve the complete concentration profiles in the lumen region.

The sequences described by Eqs. (68) and (69) converge if a Lipzchitz condition is satisfied by both equations [35,36]. Convergence is usually obtained for typical values of the model parameters and for a wide variety of differentiable kinetic equations as will be analyzed below.

For integration purposes, the use of uniform rectangular grids in the ρ, ξ-space is simple, but not suitable for the simulation of HFBRs operating in reaction regimes controlled by the mass diffusion rate, i.e., $Ge\,Pe < 1$ and/or $\Phi^2 > 1$. In such case, a rapid depletion of the substrate can take place near the inner tube entrance and/or the membrane wall on the spongy matrix side, as shown in Fig. 3. Then, if the number of grid points is not large enough the numerical integration cannot be sufficiently accurate. However, the use of enough grid points will be prohibitively demanding computer memory space and with computation times unacceptably large. For example, the total number of grid points used in ξ-space essentially depends upon the value of the parameter $Ge\,Pe$. In Table 1, results obtained with different mesh sizes are compared with those accepted as the exact solution,

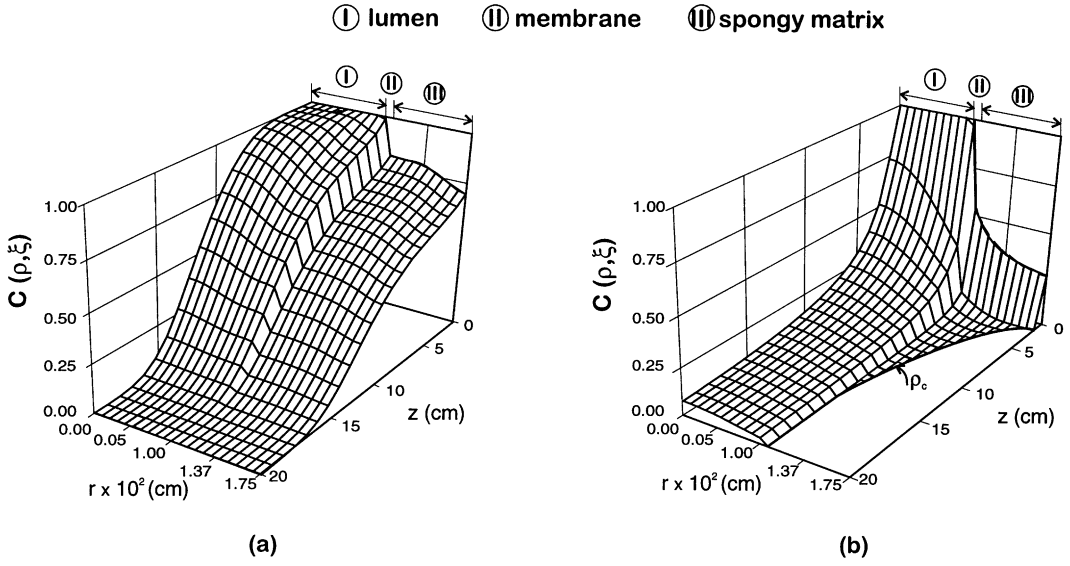

Fig. 3. Distribution of the substrate concentration in the lumen and spongy matrix regions: (a) Michaelis–Menten kinetics ($\Phi^2 = 1$ and $K_{\mathrm{M}} = 1\,\mathrm{mol\,cm^{-3}}$), and (b) zero-order kinetics ($\Phi^2 = 1$) ($D^{\mathrm{I}} = 1.0 \times 10^{-5}\,\mathrm{cm^2\,s^{-1}}$, $D^{\mathrm{II}} = 1.0 \times 10^{-6}\,\mathrm{cm^2\,s^{-1}}$, $D^{\mathrm{III}} = 1.0 \times 10^{-5}\,\mathrm{cm^2\,s^{-1}}$, $Ge\,Pe = 0.125$, $K^a = 1$, $K^b = 1$, $a = 1.00 \times 10^{-2}\,\mathrm{cm}$, $b = 1.05 \times 10^{-2}\,\mathrm{cm}$, $d = 1.75 \times 10^{-2}\,\mathrm{cm}$, $L = 2 \times 10^{1}\,\mathrm{cm}$).

Table 1
Errors relative to the exact solution in terms of the *Ge Pe* parameter for different mesh sizes[a]

Ge Pe	Relative error (%)						
	50 meshes	100 meshes	200 meshes	400 meshes	600 meshes	800 meshes	1000 meshes
(a) *Percentage error in predictions of the substrate concentration at the membrane wall on the lumen side at* $\xi = 0.1$							
0.50	8.47	5.15	2.97	1.41	0.72	0.29	0.00
1.00	6.99	4.35	2.53	1.22	0.62	0.27	0.00
2.00	5.61	3.53	2.06	0.99	0.50	0.20	0.00
4.00	4.40	2.76	1.58	0.73	0.35	0.14	0.00
(b) *Percentage error in predictions of the substrate averaged bulk concentration on the lumen side at* $\xi = 0.1$							
0.50	0.55	0.05	0.18	0.14	0.08	0.04	0.00
1.00	0.49	0.10	0.02	0.04	0.03	0.01	0.00
2.00	0.34	0.10	0.02	0.00	0.00	0.00	0.00
4.00	0.20	0.07	0.02	0.00	0.00	0.00	0.00

[a] $D^{\mathrm{I}} = 1.0 \times 10^{-5}\,\mathrm{cm^2\,s^{-1}}$, $D^{\mathrm{II}} = 1.0 \times 10^{-6}\,\mathrm{cm^2\,s^{-1}}$, $Ge\,Pe = 0.5$, $K^a = 1$, $K^b = 1$, $H = 2.0$, $n = 1$, $a = 1.00 \times 10^{-2}$ cm, $b = 1.05 \times 10^{-2}$ cm, $d = 1.75 \times 10^{-2}$ cm, $L = 2 \times 10^{1}$ cm.

which are achieved with a fixed axial grid containing 1000 meshes. It is noticeable that a workable mesh size in a personal computer, for example 200 meshes, only provides an acceptable agreement with the exact solution for values of *Ge Pe* greater than 1. However, for the same number of grid points, non-uniform grids give more accurate results. Then the mentioned limitation can be overcome using a continuous transformation of the ξ-coordinate and the numerical integration can be done on a uniform rectangular grid in the transformed space. A similar approach can be applied to transform the ρ-coordinate in the spongy matrix region.

5.2. Grid transformations

Several techniques for grid generation and the use thereof in the numerical solution of differential equations have been proposed to obtain grid points closely spaced in regions with steep gradients and widely spaced where the changes are smooth [37–39]. We have found that the following transformations are quite suitable to solve the derived integral equations:

1. In the lumen region, a new ζ-coordinate can be suitably related to the original ξ-coordinate through the following equation:

$$\xi = 1 - \frac{\tanh\left[(1-\zeta)\tanh^{-1}\sqrt{1-\alpha_\zeta}\right]}{\sqrt{1-\alpha_\zeta}} \tag{70}$$

   where $0 \le \xi \le 1$, $0 \le \zeta \le 1$, and α_ζ is an adjustable parameter ranging between 0 and 1 [37]. Note that when α_ζ is equal to 1, Eq. (70) reduces to the identity transformation $\xi = \zeta$. According to this transformation, uniform mesh sizes in ζ-coordinate have grid points in ξ-coordinate closely spaced near the entrance of the inner tube and widely spaced far from that, as shown in Fig. 4a.
2. In the spongy matrix region, the new φ-coordinate to be related with the original ρ-coordinate is given by the

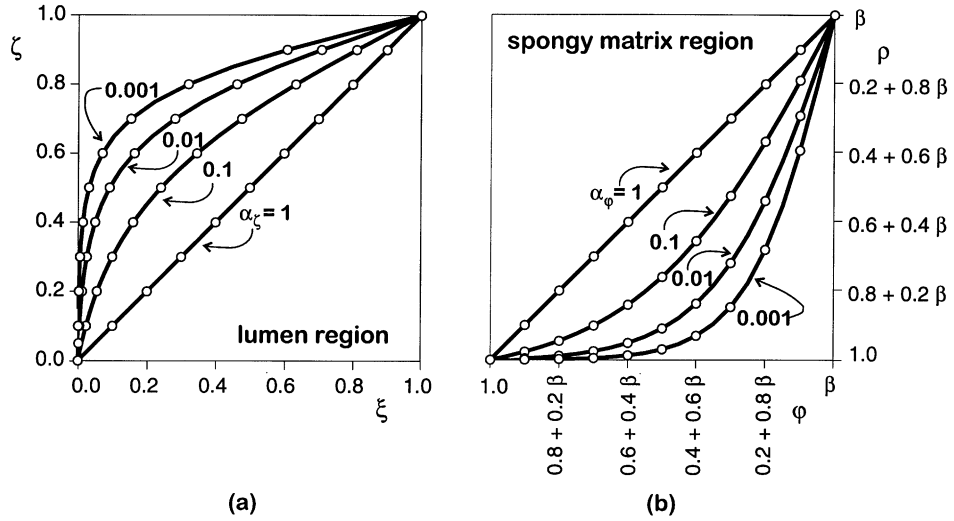

Fig. 4. Coordinate transformations for the integral equations governing the species mass balances: (a) in the lumen region, and (b) in the spongy matrix region.

following transformation:

$$\rho = 1 + \beta \left\{ 1 - \frac{\tanh\left[(1-\varphi)\tanh^{-1}\sqrt{1-\alpha_\varphi}\right]}{\sqrt{1-\alpha_\varphi}} \right\} \quad (71)$$

where $1 \le \rho \le \beta$, $1 \le \varphi \le \beta$, and α_φ is an adjustable parameter ranging between 0 and 1. If α_φ is equal to 1, Eq. (71) reduces to the identity transformation $\rho = \varphi$. Unlike the previous choice, this transformation produces a continuous stretching of the mesh size in ρ-coordinate at the vicinity of the membrane on the spongy matrix side, as illustrated in Fig. 4b. It is noticeable that the smaller the α_φ and α_ζ values become, the higher the stretching results.

5.3. Transformed integral equations

The governing integral equations are now subjected to the proposed transformations. According to the transformation defined by Eq. (70), Eq. (26) in ρ, ζ-space becomes

$$\begin{aligned} C^{\mathrm{I}}(\rho,\zeta) = {} & \left[\sum_1^\infty \frac{\phi_n(1)\phi_n(\rho)}{A_n^2\lambda_n^2} - \left(\rho^2 - \frac{1}{4}\rho^4 - \frac{7}{24}\right) \right] \\ & \times H[C^{\mathrm{I}}(1,\zeta) - KC^{\mathrm{III}}(1,\zeta)] \\ & + \int_0^1 \mathrm{d}\bar{\rho}\, \bar{\rho}(1-\bar{\rho}^2) G^{\mathrm{I}}(\rho,\zeta/\bar{\rho},0) C^{\mathrm{I}}(\bar{\rho},0) \\ & - \frac{1}{2\,Ge\,Pe} \int_0^\zeta \mathrm{d}\bar{\zeta}\, J_\zeta G^{\mathrm{I}}(\rho,\zeta/1,\bar{\zeta}) H[C^{\mathrm{I}}(1,\bar{\zeta}) \\ & - KC^{\mathrm{III}}(1,\bar{\zeta})] \end{aligned} \quad (72)$$

then

$$\begin{aligned} C^{\mathrm{I}}(1,\zeta) = {} & \left[\sum_1^\infty \frac{\phi_n^2(1)}{A_n^2\lambda_n^2} - \frac{11}{24} \right] H[C^{\mathrm{I}}(1,\zeta) - KC^{\mathrm{III}}(1,\zeta)] \\ & + \int_0^1 \mathrm{d}\bar{\rho}\, \bar{\rho}(1-\bar{\rho}^2) G^{\mathrm{I}}(1,\zeta/\bar{\rho},0) C^{\mathrm{I}}(\bar{\rho},0) \\ & - \frac{1}{2\,Ge\,Pe} \int_0^\zeta \mathrm{d}\bar{\zeta}\, J_\zeta G^{\mathrm{I}}(1,\zeta/1,\bar{\zeta}) H[C^{\mathrm{I}}(1,\bar{\zeta}) \\ & - KC^{\mathrm{III}}(1,\bar{\zeta})], \quad 0 \le \zeta \le 1 \text{ and } 0 \le \bar{\zeta} \le 1 \end{aligned} \quad (73)$$

where the integration is now realized by taking equal increments in ζ-coordinate, instead of ξ-coordinate, and the Jacobian J_ζ is given by

$$J_\zeta = \frac{\tanh^{-1}\sqrt{1-\alpha_\zeta}\,\operatorname{sech}^2\left[(1-\zeta)\tanh^{-1}\sqrt{1-\alpha_\zeta}\right]}{\sqrt{1-\alpha_\zeta}} \quad (74)$$

According to Eq. (71), Eq. (44) in φ, ξ-space becomes

$$\begin{aligned} C^{\mathrm{III}}(\varphi,\xi) = {} & G^{\mathrm{III}}(\varphi/1) HC^{\mathrm{I}}(1,\xi) \\ & + \nu \int_1^\beta \mathrm{d}\bar{\varphi}\, J_\varphi \bar{\varphi} G^{\mathrm{III}}(\varphi/\bar{\varphi}) \Omega^{\mathrm{III}}(\mathbf{C}(\bar{\varphi},\xi)), \\ & 1 \le \bar{\varphi} \le \beta \end{aligned} \quad (75)$$

with

$$\begin{aligned} C^{\mathrm{III}}(1,\xi) = {} & G^{\mathrm{III}}(1/1) HC^{\mathrm{I}}(1,\xi) \\ & + \nu \int_1^\beta \mathrm{d}\bar{\varphi}\, J_\varphi \bar{\varphi} G^{\mathrm{III}}(1/\bar{\varphi}) \Omega^{\mathrm{III}}(\mathbf{C}(\bar{\varphi},\xi)), \\ & 1 \le \bar{\rho} \le \beta \end{aligned} \quad (76)$$

respectively, where the integration is now realized by taking equal increments in φ-coordinate instead of ρ-coordinate. The Jacobian J_φ is given by

$$J_\varphi = \frac{\beta \tanh^{-1}\sqrt{1-\alpha_\varphi}\,\operatorname{sech}^2\left[(1-\varphi)\tanh^{-1}\sqrt{1-\alpha_\varphi}\right]}{\sqrt{1-\alpha_\varphi}} \quad (77)$$

5.4. Numerical exploitation

Eqs. (73) and (76) were solved through the iterative procedure proposed in Section 5.1 until relative errors smaller than 10^{-4} were achieved. A simple equispaced quadrature algorithm, such as the Newton $\frac{3}{8}$ method, was used to perform the numerical integration. All calculations were performed in double precision arithmetic.

Fig. 5a and b shows the axial profiles of the substrate concentration at the membrane wall on the lumen side and the averaged bulk concentration, both in a region near to the entrance of the HFBR, for two typical values of the parameter *Ge Pe*. Results obtained by solving Eqs. (73) and (75) with a workable number of mesh points (grids with 200 meshes and $\alpha_\zeta = 0.1, 0.5$ and 1.0) are compared with those which can be accepted as the exact solution (fixed grid with 1000 meshes). There are significant deviations between the predicted values with a fixed grid with 200 meshes ($\alpha_\zeta = 1$) and the exact values obtained with 1000 meshes ($\alpha_\zeta = 1$). It is apparent that the lower the value of *Ge Pe*, the greater the deviations become. Then the computation would be done on a very refined equispaced grid in ξ-space. However, the use of grids with more than 250 meshes is not practical since achieving the solution requires excessive computational effort and computer memory space. The transformation given by Eq. (70) allows us to overcome such difficulties. In fact, the continuous variable grid method with 200 meshes and $\alpha_\zeta \le 1 \times 10^{-1}$ predicts concentration profiles similar or equal to those which are achieved with 1000 meshes, as shown in Fig. 5a and b. For the case analyzed, the optimal value of parameter α_ζ was found to be around 1×10^{-1} and essentially depends on the value of *Ge Pe*. After considerable number of attempts, we proposed to choose α_ζ according to the following relationship:

$$\alpha_\zeta = \begin{cases} 1 & \text{for } Ge\,Pe \ge 2 \\ 0.2\,Ge\,Pe & \text{for } Ge\,Pe < 2 \end{cases} \quad (78)$$

In the spongy matrix region, the advantages of using the transformation given by Eq. (71) was corroborated. It was found that the simplest choice of α_φ in terms of the parameter

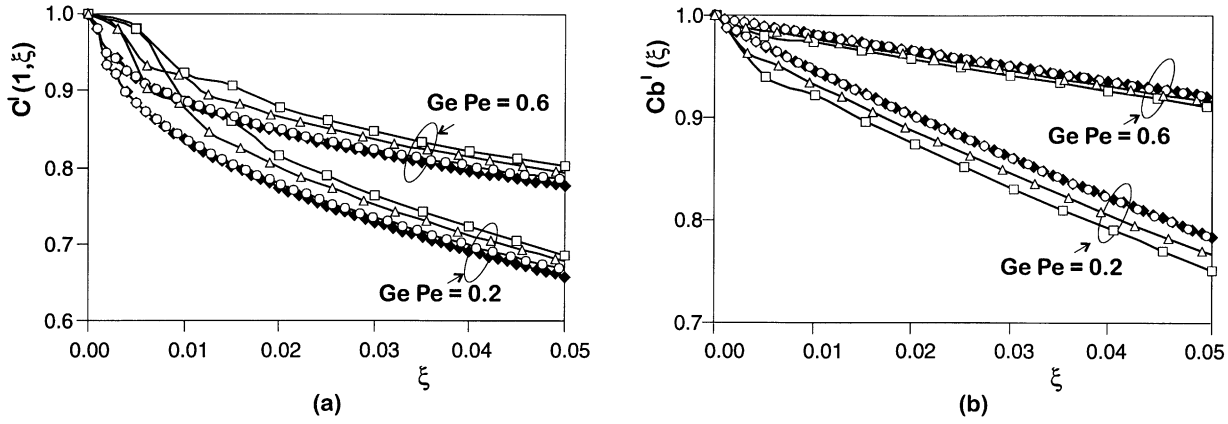

Fig. 5. Predicted axial profiles: (a) substrate concentration at the membrane wall on the lumen side, and (b) averaged bulk concentration. The profiles correspond to $Pe = 400$ and 1200, $Ge = 5 \times 10^{-4}$, $H = 2$, $K = 1$ and $\Phi^2 = 1$. (◆) exact value with $\alpha_\xi = 1$ and 1000 meshes; (□) $\alpha_\xi = 1$ and 200 meshes; (△) $\alpha_\xi = 0.5$ and 200 meshes; and (○) $\alpha_\xi = 0.1$ and 200 meshes.

of the model which governs the concentration profiles in this region is given by

$$\alpha_\varphi = \begin{cases} 1 & \text{for } \Phi^2 \leq 1 \\ 1/\Phi^2 & \text{for } \Phi^2 > 1 \end{cases} \tag{79}$$

6. Applications and performance of the numerical method

For all calculations presented herein, $a = 100\,\mu$, $b = 105\,\mu$, $d = 175\,\mu$, $Re \leq 1500$, $250 \leq Pe \leq 1200$, $10^{-4} \leq Ge \leq 10^{-3}$, $5 \times 10^{-1} \leq H \leq 8$, and $10^{-1} \leq \Phi^2 \leq 10$. This set of values is in accordance with the model assumptions and covers typical operating conditions for HF-BRs. In order to fulfil the assumption (i), the length of the lumen region flow before the spongy matrix was estimated to be less than 1 cm because the parabolic axial velocity profile is fully developed for an entrance length $L_e \leq 5.75 \times 10^{-2} \times 2a\,Re$ [40]. The assumption (ii) is fulfilled whenever the convective transport is two orders of magnitude greater than the axial diffusive transport. In mathematical terms, it means $2\,Pe(1-\rho^2) \geq 10^2\,Ge$, which in the range $0 \leq \rho \leq 0.999$ is nearly satisfied for $Pe \geq 250$ and $Ge \leq 10^{-2}$. In the practice, it might be that the radial convective transport will be no null. However, it is to be hoped that the assumption (iii) be acceptable in accordance with the fact that the radial convective transport can be still neglected with respect to the radial diffusive flux for upper bounds of the radial Peclet number [9]. Assumptions (v) and (viii) are made to reduce computational efforts, but there are no restrictions other than the usual ones on the dependence of the physical properties. The validity of assumptions (vi), (vii) and (ix) will particularly depend on the permeable membrane and spongy matrix characteristics. A comprehensive analysis on this matter can be found elsewhere [9].

6.1. Power-law kinetics

The more simplified representation for the substrate reaction rate is the power-law model

$$\Omega^{\mathrm{III}}(\mathbf{C}(\rho,\xi)) = \Phi^2 C^{\mathrm{III}}(\rho,\xi)^n \tag{80}$$

where the dimensionless reaction rate is expressed in terms of the Thiele number and the reaction order ($n < 0$). Particularly, the first-order limit of the Michaelis–Menten kinetics has been typically used to describe enzymatic reaction rates [7,8,41–44].

The performance of the computational method was analyzed covering a wide range of operating conditions and reaction orders. For all the values explored, the calculation times to achieve a specified accuracy are reduced by almost an order of magnitude if the transformed grid method is used instead of a fixed grid in the original ρ,ξ-space. Convergence is ensured when the Lipzchitz condition is satisfied. For Eq. (75) with first-order kinetics, the Lipzchitz condition becomes

$$\frac{1}{\Phi^2} > \frac{(1+\beta)^2}{2}\ln(1+\beta) + ((1+\beta)^2 - 1)\left(\frac{1}{2HK} - \frac{1}{4}\right) \tag{81}$$

This means that the convergence is surely obtained when the overall rate of the process is controlled by the chemical reaction, i.e., when either the diffusional resistance in the spongy matrix is negligible ($\Phi^2 < 1$), the spongy matrix is thin ($\beta \rightarrow$ small value), the coefficient of mass transfer through the membrane or the partition coefficients are high ($HK > 1$). The condition given by Eq. (81) was numerically corroborated, as illustrated in Fig. 6a–c. For all analyzed values of H and $Ge\,Pe > 1$, the convergence domains (lower-left) are exactly described by Eq. (81) since the convergence is governed by Eq. (75). For $Ge\,Pe < 0.25$ the convergence domains begins to be governed by Eq. (73) for which, unlike Eq. (75), an explicit expression to predict

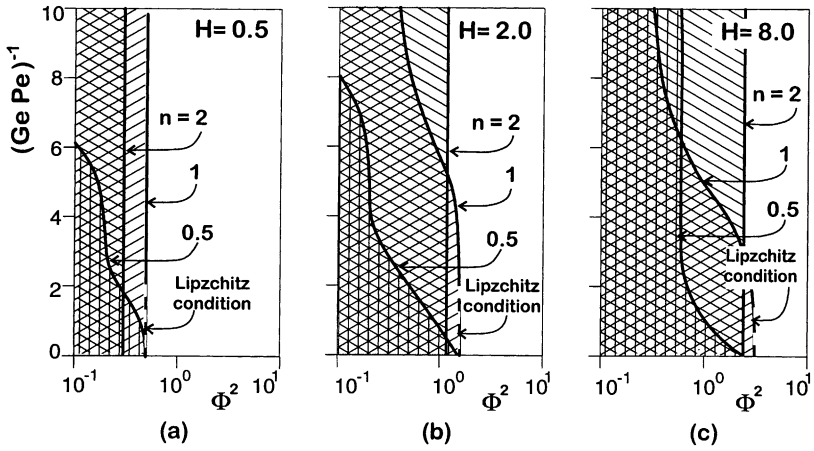

Fig. 6. Convergence domains (lower-left regions) for power-law kinetics. The border lines correspond to half-order ($n = 0.5$), first-order ($n = 1$) and second-order ($n = 2$) kinetics. The dashed lines indicate the limits predicted by the Lipzchitz condition for the first-order kinetics.

the convergence conditions cannot be obtained. The convergence domains are then completed by computational experimentation. Likewise, Fig. 6a–c shows the convergence maps corresponding to half-order and two-order kinetics. It is noticeable that the convergence domains broaden when the membrane resistance is lower and the reaction order is higher. The convergence domains significantly reduce for operating conditions leading to a process rate significantly controlled by diffusive mass transport in the lumen, membrane and spongy matrix regions, but such combination of conditions is either unusual or undesirable in practical applications because the effectiveness of the HFBR becomes excessively low.

6.2. Michaelis–Menten kinetics

The kinetics for enzymatic reactions are usually expressed on the basis of the general formulation given by Michaelis–Menten:

$$\Omega^{\mathrm{III}}(\mathbf{C}(\rho,\xi)) = \frac{\Phi^2 C^{\mathrm{III}}(\rho,\xi)}{1 + (c^0/K_{\mathrm{M}})C^{\mathrm{III}}(\rho,\xi)} \tag{82}$$

which resembles that suggested by Langmuir for surface catalysis. Significant analyses of HFBRs with Michaelis–Menten kinetics have been published elsewhere [5,8,23,42,45–47].

Fig. 7a–c illustrate the convergence domains for a wide range of values of the kinetic parameters. It is apparent that the convergence can be achieved in a domain wider than the one obtained for first-order kinetics. In regions close to the convergence limits, the results have repeatedly shown high-gradients of concentration which severely restrict the substrate available to the cells, the reaction conditions becoming vastly inadequate. From a practical viewpoint, non-convergence domains coincide with unacceptable specifications of the HFBR system. For the most demanding conditions, the computing times obtained with the transformed grid method become nearly one order of magnitude smaller than the corresponding one to fixed grids in

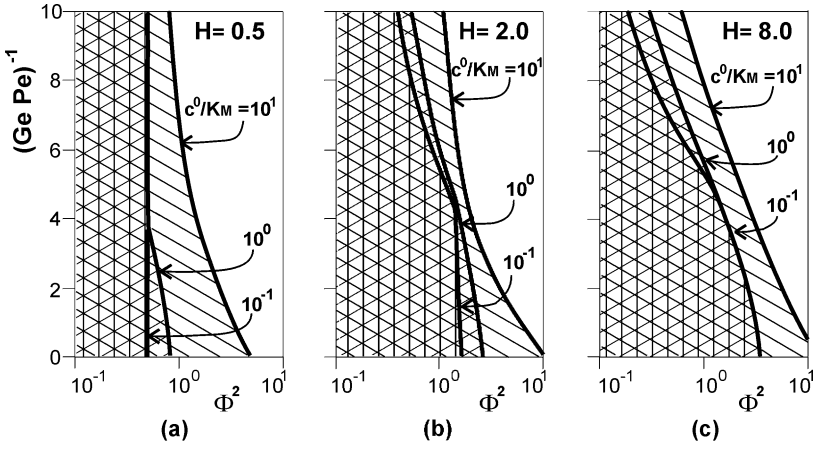

Fig. 7. Convergence domains (lower-left regions) for Michaelis–Menten kinetics. The border lines indicate the limits for different values of the c^0/K_{M} parameter.

ρ, ξ-space, as mentioned in Section 5.4. The convergence maps can be used to know a priori the feasibility to implement iterative schemes of sure and fast convergence.

6.3. Zero-order kinetics

Some enzymatic reactions can be approximated as zero-order reactions. While the substrate concentration remains finite, the non-dimensional kinetic equation becomes independent of the concentration:

$$\Omega^{\mathrm{III}}(\mathbf{C}(\rho,\xi)) = \Phi^2 \tag{83}$$

but as long as the substrate concentration drops to zero — at the so-called critical radius — the local reaction rate becomes zero. Theoretical analysis of HFBRs with zero-order kinetics as limiting form of the Michaelis–Menten kinetics can be found in several contributions [8,15,41,42].

The values of the critical radius can be obtained as roots of the following implicit equation:

$$\begin{aligned} &1 + \nu\Phi^2 K\left\{\frac{1}{2HK}[\rho_c^2 - 1] - \frac{1}{4}[\rho_c^2 - 1] + \frac{\rho_c^2}{2}\ln\rho_c\right\} \\ &\quad + \nu\Phi^2\frac{\rho_c^2 - 1}{2} \\ &\quad \times\left\{\frac{11}{24} + \frac{2}{Ge\,Pe}\xi - \sum_1^\infty \frac{\phi_n^2(1)}{A_n^2\lambda_n^2}\exp\left(-\frac{\lambda_n^2}{2\,Ge\,Pe}\xi\right)\right\} \\ &\quad = 0 \end{aligned} \tag{84}$$

which was derived as particular case of Eq. (45). The subroutine ZSPOW of the IMSL library has proved to be effective to solve Eq. (84). The algorithm is a variation of the Newton method and takes precautions to avoid large step sizes or increasing residuals [48].

Once the values of the critical radius are known, the concentration profiles can be obtained without having to resort to an iterative scheme of numerical solution.

Case (a). When the substrate concentration remains greater than zero throughout the spongy matrix (i.e., where $\rho_c \geq \beta$), the following explicit equations must be solved:

$$\begin{aligned} C^{\mathrm{I}}(\rho,\xi) &= 1 + \nu\Phi^2\frac{\beta^2 - 1}{2}\left\{\rho^2 - \frac{1}{4}\rho^4 - \frac{7}{24} + \frac{2}{Ge\,Pe}\xi\right. \\ &\quad \left. - \sum_1^\infty \frac{\phi_n(\rho)\phi_n(1)}{A_n^2\lambda_n^2}\exp\left(-\frac{\lambda_n^2}{2\,Ge\,Pe}\xi\right)\right\} \end{aligned} \tag{85}$$

and

$$\begin{aligned} C^{\mathrm{III}}(\rho,\xi) &= \frac{1}{K}C^{\mathrm{I}}(1,\xi) + \nu\Phi^2 \\ &\quad \times\left\{\frac{1}{2HK}[\beta^2 - 1] - \frac{1}{4}[\rho^2 - 1] + \frac{\beta^2}{2}\ln\rho\right\} \end{aligned} \tag{86}$$

Case (b). When the substrate concentration depleted before reaching the shell wall (i.e., where $\rho_c < \beta$), the following explicit equations must be used:

$$\begin{aligned} C^{\mathrm{I}}(\rho,\xi) &= 1 + \nu\Phi^2\frac{\rho_c^2 - 1}{2}\left\{\rho^2 - \frac{1}{4}\rho^4 - \frac{7}{24} + \frac{2}{Ge\,Pe}\xi\right. \\ &\quad \left. - \sum_1^\infty \frac{\phi_n(\rho)\phi_n(1)}{A_n^2\lambda_n^2}\exp\left(-\frac{\lambda_n^2}{2\,Ge\,Pe}\xi\right)\right\} \end{aligned} \tag{87}$$

and

$$C^{\mathrm{III}}(\rho,\xi) = \Theta(\rho_c - \rho)\nu\Phi^2\left\{\frac{1}{4}[\rho_c^2 - \rho^2] + \frac{\rho_c^2}{2}\ln\frac{\rho}{\rho_c}\right\} \tag{88}$$

Numerical computations are very fast as corroborated by an extensive numerical exploitation. Nevertheless, it seems

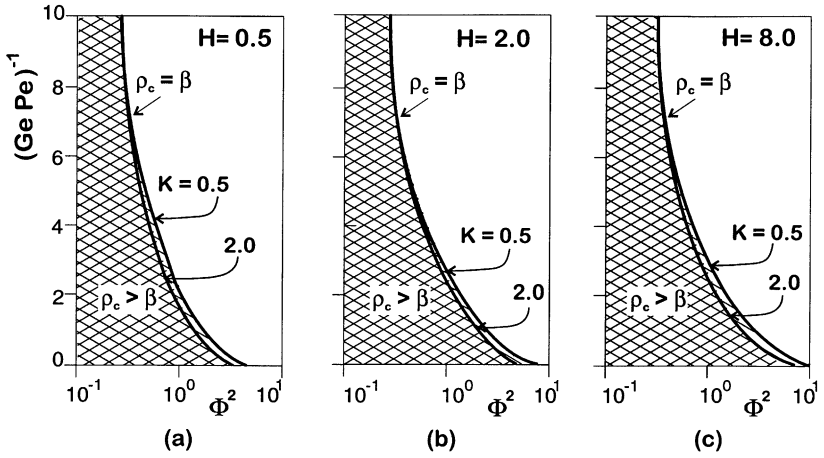

Fig. 8. Maps showing the domains (left regions) for which the substrate concentration remains greater than zero everywhere inside the spongy matrix for zero-order kinetics. The border lines indicate the limits for different values of the lumen/spongy matrix partition coefficient.

convenient to present maps in terms of the HFBR parameters showing if the substrate concentration can be depleted before reaching the shell wall, and thus knowing a priori if Eq. (84) must be solved. Results of numerous computations are shown in Fig. 8a–c on which the operation point can be located according to the operating conditions to be analyzed. If the operation point is located within the corresponding dashed region, the substrate concentration remains greater than zero everywhere inside the spongy matrix, and then only Eqs. (85) and (86) must be solved. Otherwise, the axial profile of the critical radius must be necessarily obtained from Eq. (84).

7. Conclusions

A formal general solution of the mass balance equations for HFBRs with any arbitrary kinetic equation was obtained by means of the Green's function method. The general solution is said formal because it is expressed in terms of implicit integral equations which require some iterative scheme of solution. The substrate remaining finite throughout the spongy matrix and the substrate exhausted before reaching the shell wall cases are both treated in systematic form using an indicator function whose values are one if the substrate concentration is finite, and zero if the substrate concentration is equal to zero. The obtained general solution renders explicit analytical forms for limiting cases, some of them have been treated in the literature.

The main advantages of the solution for the substrate concentration lies in the following facts: (i) on the lumen side, Green's functions are expressed in terms of an eigenvalue problem which depends neither on the particular conditions of the laminar flow nor on the coefficients of mass transfer through the permeable membrane, so that once eigenvalues are calculated, they become a result which does not vary from one application to another; (ii) on the spongy matrix side, Green's functions do not depend on the kinetic equation, this avoids repetitive computational effort when treating different reaction kinetics; (iii) the resulting format of integral equations is apt to devise a numerical solution based on a simple iterative process along the permeable wall and through the spongy matrix, without having to resort to the complete concentration profiles in the lumen, which yield to iterative schemes of fast convergence; and (iv) zero-order kinetics are treated as a particular case of the general solution which lead to an unmatched expression in terms of the critical radius and operative parameters of the HFBR, from which it is possible to calculate the critical radius in a fast, direct, reliable manner using the proposed numerical algorithms. Once the values of the critical radius are known, the substrate concentration profiles in the lumen and spongy matrix can be straightaway obtained from explicit analytical equations.

The numerical procedure can adequately handle problems with steep axial and radial gradients of concentration in the lumen and spongy matrix regions, respectively. In regard to implementation, an improvement of the accuracy of the solution without wasting computer memory space and running time was obtained with the transformed grid method using hyperbolic tangent functions. The method can be extendible to other continuous transformations by the simple substitution of the corresponding Jacobian expression in Eqs. (72), (73), (75) and (76). Then, the computation can be done on a fixed uniform grid using standard techniques of integration. The convergence of the iterative procedure can be achieved for a wide range of operating conditions having practical importance. The results presented herein demonstrate the effectiveness of this approach for the simulation of HFBRs with power-law, Michaelis–Menten and zero-order kinetics; however it is readily extendible to any arbitrary functional form of the kinetic equation.

Acknowledgements

Support from the Consejo Nacional de Investigaciones Científicas y Técnicas (CONICET) and from the Universidad Nacional del Litoral of Argentina is gratefully acknowledged.

References

[1] R.A. Knazek, P.M. Guillino, P.O. Kohler, R.L. Dedrick, Cell-culture on artificial capillaries. Approach to tissue growth in vitro, Science 178 (1972) 65.
[2] G. Belfort, Membranes and bioreactors: a technical challenge in biotechnology, Biotechnol. Bioeng. 33 (1989) 1047–1066.
[3] P.S. Sehanputri, C.G. Hill Jr., Biotechnology for the production of nutraceuticals enriched in conjugated linoleic acid. I. Uniresponse kinetics of the hydrolysis of corn oil by a *Pseudomonas* sp. lipase immobilized in hollow fiber reactors, Biotechnol. Bioeng. 64 (5) (1999) 568–579.
[4] J.E. Dowd, I. Weber, B. Rodriguez, J.M. Piret, K.E. Kwok, Predictive control of hollow-fiber bioreactors for the production of monoclonal antibodies, Biotechnol. Bioeng. 63 (4) (1999) 484–492.
[5] J.D. Brotherton, P.C. Chau, Modeling of axial-flow hollow fiber cell culture bioreactors, Biotecnol. Prog. 12 (5) (1996) 575–590.
[6] L.R. Waterland, A.S. Michaels, C.R. Robertson, A theoretical model for enzymatic catalysis using asymmetric hollow fiber membranes, AIChE J. 20 (1) (1974) 50–59.
[7] S.S. Kim, D.O. Cooney, An improved theoretical model for hollow fiber enzymatic reactors, Chem. Eng. Sci. 31 (1976) 289–294.
[8] I.A. Webster, M.L. Schuler, Mathematical models for hollow fiber enzyme reactors, Biotech. Bioeng. 20 (10) (1978) 1541–1556.
[9] J.M. Piret, C.L. Cooney, Model of oxygen transport limitations in hollow fiber bioreactors, Biotechnol. Bioeng. 37 (1991) 80–92.
[10] M.E. Davis, J. Yamanis, Analysis of annular bed reactor for methanation of carbon-monoxide, AIChE J. 28 (2) (1982) 266–273.
[11] M.E. Davis, J. Yamanis, Axial dispersion in the annular bed reactor, Chem. Eng. Commun. 25 (1984) 1–10.
[12] H. Beyenal, A. Tanyolaç, A mathematical model for hollow fiber biofilm reactors, Chem. Eng. J. 56 (1994) B53–B59.
[13] M.E. Davis, L.T. Watson, Mathematical modeling of annular reactors, Chem. Eng. J. 33 (1986) 133–142.
[14] V.K. Jayaraman, The solution of hollow fiber bioreactor design equations, Biotechnol. Prog. 8 (1992) 462–464.

[15] V.K. Jayaraman, Solution of hollow fiber bioreactor design equations for zero-order limit of Michaelis–Menten kinetics, Chem. Eng. J. 51 (1993) B63–B66.
[16] V.K. Jayaraman, Solution of hollow fiber bioreactor design equations: the case of power-law fluids, Chem. Eng. J. 55 (1994) B73–B75.
[17] R.N. Paunovic, Z.Z. Zavargo, M.N. Tekic, Analysis of a model of hollow-fiber bioreactor wastewater treatment, Chem. Eng. Sci. 48 (6) (1993) 1069–1075.
[18] C. Kleinstreuer, S.S. Agarwal, Analysis and simulation of hollow-fiber bioreactor dynamics, Biotechnol. Bioeng. 28 (1986) 1233–1240.
[19] J. Koska, B.D. Bowen, J.M. Piret, Protein transport in packed-bed ultrafiltration hollow-fibre bioreactors, Chem. Eng. Sci. 52 (14) (1997) 2251–2263.
[20] R.A. Kumar, J.M. Modak, Transient analysis of mammalian cell growth in hollow fibre bioreactors, Chem. Eng. Sci. 52 (12) (1997) 1845–1860.
[21] D.G. Taylor, J.M. Piret, B.D. Bowen, Protein polarization in isotropic membrane hollow-fiber bioreactors, AIChE J. 40 (2) (1994) 321–333.
[22] C. Heath, G. Belfort, Immobilization of suspended mammalian cells: analysis of hollow fiber and microcapsule bioreactors, Adv. Biochem. Eng./Biotechnol. 34 (1987) 1–31.
[23] R.J. Grau, A.E. Cassano, H.A. Irazoqui, Mass transfer through permeable walls: a new integral equation approach for cylindrical tubes with laminar flow, Chem. Eng. Commun. 64 (1988) 47–65.
[24] P. Arce, An integral-spectral formulation for convective–diffusive transport in a packed-bed with adsorption at the wall and bulk reaction, Chem. Eng. Commun. 138 (1995) 113–125.
[25] R.J. Grau, M.I. Cabrera, A.E. Cassano, The laminar flow tubular reactor with homogeneous and heterogeneous reactions. I. Integral equations for diverse reaction rate regimes, Chem. Eng. Commun., in press.
[26] M.I. Cabrera, R.J. Grau, A.E. Cassano, The laminar flow tubular reactor with homogeneous and heterogeneous reactions. II. Application to reactor modeling involving free radical reactions, Chem. Eng. Commun., in press.
[27] H. Cantero, R.J. Grau, M.A. Baltanás, Cocurrent turbulent tube reactor with multiple gas injections and recycle of slurry: a treatment in terms of Green's functions, Comput. Chem. Eng. 18 (7) (1994) 551–561.
[28] P. Arce, B.R. Locke, I.M.B. Trigatti, An integral-spectral approach for reacting Poiseuille flows, AIChE J. 42 (1) (1996) 23–41.
[29] Z. Chen, P. Arce, B.R. Locke, Convective–diffusive transport with a wall reaction in Couette flows, Chem. Eng. J. 61 (1996) 63–71.
[30] Z. Chen, P. Arce, An integral-spectral approach for convective–diffusive mass transfer with chemical reaction in Couette flow. Mathematical formulation and numerical illustration, Chem. Eng. J. 68 (1997) 11–27.
[31] P.E. Arce, A.E. Cassano, H.A. Irazoqui, The tubular reactor with laminar flow regime: an integral equation approach. I. Homogeneous reaction with arbitrary kinetics, Comput. Chem. Eng. 12 (11) (1988) 1103–1113.
[32] M. Abramowitz, I.A. Stegun, Handbook of Mathematical Functions, Dover, New York, 1965.
[33] P.A. Dirac, The Principles of Quantum Mechanics, 4th Edition, Oxford University Press, Oxford, 1958.
[34] B. Tabis, A method of calculation for tubular reactors using a Green's function, Int. Chem. Eng. 27 (1987) 539–544.
[35] E.A. Coddington, N. Levinson, Theory of Ordinary Differential Equations, McGraw-Hill, New York, 1955.
[36] M. Guzman, Real Variable Methods in Fourier Analysis, North-Holland, Amsterdam, 1981.
[37] A.K. Agrawal, R.S. Peckover, Nonuniform grid generation for boundary-layer problems, Comput. Phys. Commun. 19 (1980) 171–178.
[38] E. Kalnay de Rivas, On the use of nonuniform grids in finite-difference equations, Comput. Phys. Commun. 10 (1972) 202–210.
[39] J.F. Thompson, Z.U.A. Warsi, C.W. Mastin, Numerical Grid Generation. Foundations and Applications, Elsevier, New York, 1985.
[40] H.L. Langhaar, Trans. Am. Soc. Mech. Eng. A 64 (1942) 55.
[41] P.R. Rony, Multiphase catalysts. 2. Hollow fiber catalysts, Biotech. Bioeng 13 (3) (1971) 431.
[42] I.A. Webster, M.L. Schuler, Whole-cell hollow-fiber reactor. Transient substrate concentration profiles, Biotech. Bioeng. 23 (2) (1981) 447–450.
[43] J.A. Schoenberg, G. Belfort, Enhanced nutrient transport in hollow fiber perfusion reactor, Biotech. Prog. 3 (1987) 80–89.
[44] R. Willaert, A. Smets, L. De Vuyst, Mass transfer limitations in diffusion-limited isotropic hollow fiber bioreactors, Biotechnol. Technol. 13 (5) (1999) 317–323.
[45] C. Horvath, L.H. Shendalwan, R.T. Light, Open tubular heterogeneous enzyme reactors. Analysis of a theoretical model, Chem. Eng. Sci. 28 (2) (1973) 375–388.
[46] C. Georgakis, P.C.H. Chan, R. Aris, Design of stirred reactors with hollow fiber catalysts for Michaeles–Menten kinetics, Biotech. Bioeng. 17 (2) (1975) 99.
[47] S.A. Benner, Enzyme kinetics and molecular evolution, Chem. Rev. 89 (1989) 789–806.
[48] J. More, B. Garbow, K. Hillstromn, Used Guide for MINPACK-1, Argonne National Laboratory Report ANL-80-74, Argonne, IL, August, 1980.